Diamond & Related Materials 170 (2026) 114302

Contents lists available at ScienceDirect

Diamond & Related Materials

journal homepage: www.elsevier.com/locate/diamond

Atomic layer etching of diamond using argon and oxygen

Alma Beatrice Sergi [a], Angelika Kaiser [a], Jakob Buchheim [a], Markus Mohr [a,*]

[a] German Aerospace Center (DLR), Institute of Quantum Technologies, Wilhelm-Runge-Straße 10, 89081, Ulm, Germany

ARTICLE INFO

Keywords:
Atomic layer etching
Surface defects
Plasma etching
Quantum technology

ABSTRACT

The ability to remove surface defects of diamond by dry etching methods is of high importance for applications that make use of shallow color centers in diamond. Here, we present an atomic layer etching process, making use of oxygen as dosing gas and argon as etching gas, in order to achieve controlled etching of the surface without creating additional defects by sputtering. We demonstrate a process window, where quasi-self-limiting atomic layer etching takes place with an etch per cycle of (1.909 ± 0.004) Å/cycle, corresponding to about 2 atomic layers of the {100} oriented diamond sample. The process is able to reduce the rms surface roughness down to (0.15 ± 0.01) nm. Furthermore, X-ray photoelectron spectroscopy indicates only a small amount of sp^2 bonded carbon on the diamond surface after the atomic layer etching process.

1. Introduction

Advanced diamond-based applications in the field of quantum computing, quantum sensing, and quantum communication are based on color centers which require a defect free diamond environment for long coherence times [1,2]. Quite often, the relevant color centers are not deep inside the bulk crystal but close to the surface, e.g. shallow NV-centers used for quantum sensing with high sensitivity and high lateral resolution [2,3]. NV-centers close to the polished diamond surface, or NV-centers close to etched structures, e.g. pillars, are prone to decoherence by influences from surface defects [4,5], as polished and plasma etched surfaces often possess subsurface damage [6–9]. Finding a process to remove diamond material without creating further damage to the diamond surface is of high importance for the realization of such applications. Surface damages caused by plasma etching of diamond was already recognized earlier [10], and plasma etching processes with reduced defect generation probability were also demonstrated already [11].

An alternative process that systematically avoids surface damages is atomic layer etching (ALE). Atomic layer etching is a multistep process for removing ultrathin layers of material, and the basic concept consists of two fundamental steps: the first one is used to modify the surface and the second one to remove the modified surface [12]. Self-limiting atomic layer etching requires a controlled dosing with gas species that modify the surface and allow the removal of atomically thin layers of the material using very low energetic bombardments under ~70 eV. This energy is far below the ion energies of about a few hundred eV of typical ICP/RIE plasma etching processes [13]. The first patent on atomic layer etching was by S. Iwamatsu [14], dating back to 1981. The first patent on plasma assisted atomic layer etching is concerned with an etching process for diamond, making use of NO_2 as dosing gas that modifies the surface, and a mixture of a noble gas and hydrogen fed through an ion gun for the removal of the modified layer [15]. However, an experimental realization of this processes is not known.

An atomic layer process for etching diamond, making use of an ICP-RIE system, was developed using Cl_2 as modifying gas and Ar as the inert gas producing the ions for the removal of the modified layer [16]. An atomic layer etching process using CF_4/Ar on diamond was developed by Régnier et al., however with a relatively low synergy [17]. Draney et al. [18] were studying computationally a process they name “ion damaged layer etching”, where, in a first step, diamond is damaged by Ar ion irradiation and subsequently, the damaged layer is etched chemically by oxygen ions or by neutral hyperthermal oxygen atoms.

Molecular dynamics simulations reveal that for all investigated incident energies of oxygen ions accelerated onto a diamond surface, the C—C bonds are dissociated and carbon atoms are etched away via the generation and desorption of gaseous carbon monoxide and carbon dioxide molecules [19]. Atomic layer etching processes working for other carbon allotropes have been shown by Kim et al. [20] and Lim et al. [21] using oxygen as dosing gas and argon as etching gas for the removal of the modified layer, on highly oriented pyrolithic graphite [20] or graphene [21]. Polystyrene polymers were etched using an atomic layer etching process by O_2 exposure and subsequent Ar plasma etching [22]. Kanarik et al. show an atomic layer etching process using O_2 plasma for

* Corresponding author.
E-mail address: markus.mohr@dlr.de (M. Mohr).

https://doi.org/10.1016/j.diamond.2026.114302
Received 30 June 2026; Received in revised form 30 September 2026; Accepted 16 October 2026
Available online 18 October 2026
0925-9635/© 2026 The Authors. Published by Elsevier B.V. This is an open access article under the CC BY license (http://creativecommons.org/licenses/by/4.0/).
Open access funding enabled and organized by Projekt DEAL.

the modification step and Ar plasma for the removal step, obtaining a high synergy of 97% on amorphous carbon films [12].

In light of this, in this work, we developed and investigated an atomic layer etching process for diamond using O_2 for dosing and Ar for etching.

2. Materials and methods

2.1. Materials

The investigated samples were electronic grade single crystal diamond grown by chemical vapor deposition, with 2.0 mm × 2.0 mm × 0.5 mm in size, obtained from Element 6. The samples were of {100} surface orientation. The crystallographic miscut was reported to be of ±3° [23], and the root mean square (rms) roughness of the sample in a 40 × 40 μm^2 region was measured by AFM to be (0.26 ± 0.02) nm.

2.2. Masking

The use of oxygen as dosing gas in the atomic layer etching process requires to employ a metal mask. We used a thermally evaporated aluminum mask as masking material. After the thermal evaporation of the aluminum, patterning was done by application of a photoresist (AZ 5214 E, spinning at 9000 rpm, baking at 110 °C for 90 s), and UV exposure through a glass mask. After an additional bake at 112 °C for 90 s, the resist was flood exposed without mask, in order to convert it into a negative tone resist, crosslinking the resist in the initially unexposed areas. After development of the resist in AZ 726 MIF (about 30 s), the aluminum was patterned by etching in a solution of H_2O:HNO_3:H_3PO_4 (1:1:8) at 50 °C for about 4 min. The photoresist mask was finally removed by a resist remover (AR 300–76), and subsequent cleaning in acetone and isopropanol was performed.

2.3. Etching

After masking the diamond samples, they were etched in a dedicated atomic layer etching device (Oxford PlasmaPro 100 Cobra 300 with ALE kit). The argon was of 6.0 quality (mti IndustrieGase AG, Neu-Ulm), and connected to the chamber by its own process gas line via a mass flow controller. The oxygen (O_2 purity 6.0, mti IndustrieGase AG, Neu-Ulm) was fed through a mass flow controller followed by fast valves (10 ms open-close response) connected to the pump exhaust and the process chamber. The O_2 process gas line could then either be switched to be directed into the process chamber (during the dosing step) or to divert the gas into the pump exhaust.

The atomic layer etching process performed in this work consists of 4 steps that are repeatedly performed. Fig. 1 shows a sketch of one representative cycle of the process. One atomic layer etching cycle consists of 1) a dosing step, where oxygen is introduced into the chamber, reacting in the ICP plasma, and modifying the sample surface; 2) a subsequent purge step, required to remove the dosing gas from the chamber, which is followed by 3) the etch step, in which the table rf generator is turned on to bombard the modified surface, and 4) a final purge step to remove the etch products from the chamber. During the whole process, we kept the ICP plasma running and the Ar flow constant. With the help of an optical emission spectrometer (OceanInsight USB4000 Miniature Spectrometer), the Ar flow, and the first purge step duration was adjusted to the dosing duration in order to obtain the lowest possible oxygen background in the plasma at the end of the first purge step.

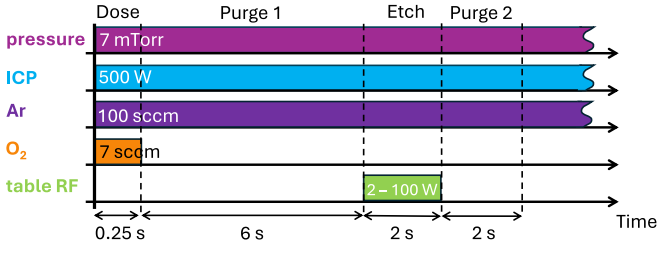


Fig. 1. Schematic of a sequence of the atomic layer etching cycle, consisting of 4 phases – Dosing, Purge 1, Etching, Purge 2, which are repeated N times. Our Oxford Cobra 300 allows the flows to be set between 0 and 100 sccm, and gas can be switched on/off with 10 ms accuracy.

A measure of the ideality of the atomic layer process is the ALE synergy S, which is defined as:

$$S\,(\%) = \frac{EPC - (\alpha + \beta)}{EPC} \times 100\% \quad (1)$$

where α and β are undesired contributions to the atomic layer etching process. The unintended etching per cycle during the dosing step is represented by α, and β represents the amount of sputtering of unmodified material in the etch step [24]. Both parameters α and β can be obtained in two separate processes: one where the etching step is removed for revealing α, and one where the dosing step is skipped for obtaining β.

For all processes performed in this work, the sample temperature was held constant at 20 °C, and the ICP power was 500 W, while the power of the table rf was varied between the etching experiments, in order to vary the ion energy of the Ar ions bombarding the diamond surface in the etching step.

2.4. Characterization

2.4.1. AFM

The etch depths, as well as the roughness measurements on the samples were performed using an atomic force microscope (Park Systems, NX10) in non-contact and tapping mode, using a standard NCHR probe. All the AFM scans were planarized and analyzed with the open-source software Gwyddion [25] and XEI (Park Systems).

2.4.2. XPS

Chemical characterization of the sample surface was performed using a commercial PHI 5800 X-ray photoelectron spectrometer from Physical Electronics. The setup was calibrated using copper (Cu). Final calibration and spectra evaluation was performed using the C 1 s C—C sp^3 at 284.8 eV. To minimize inhomogeneous surface charging, the inbuilt charge neutralization system was used. Aperture size was set to 2.0 × 0.6 mm^2. Pass energy was set to 29 eV. Survey spectra and high-resolution spectra were recorded at bulk sensitive detection angle $\theta_1 = 45°$, and at surface sensitive detection angle $\theta_2 = 70°$. Recorded data was representative for ~7 nm depth and ~ 3 nm depth of the diamond surface, respectively, and was used for angle-resolved analysis. Evaluation was performed by using CasaXPS [26].

3. Results

Fig. 2 shows the determined etch per cycle (EPC) for the variation of the table rf power, and consequently the variation of the occurring bias voltage. For all data points, 600 cycles were performed, and the etch depth was obtained by AFM measurements. The error bars for the EPC reflect the uncertainty in obtaining the etch depth from the AFM measurements, and the error bars of the bias voltage reflect the variations of the measured bias voltage value during the etching cycles. The mask erosion calculated from comparing AFM measurements before etching (mask thickness), after etching (etched depth together with the mask thickness) and after removal of the mask (etched depth) is negligible.

The variation of the table rf power revealed 3 distinct regimes. In the first regime (below about 45 V bias), we obtain an incomplete removal of the modified surface. In the second regime (between about 45 V and

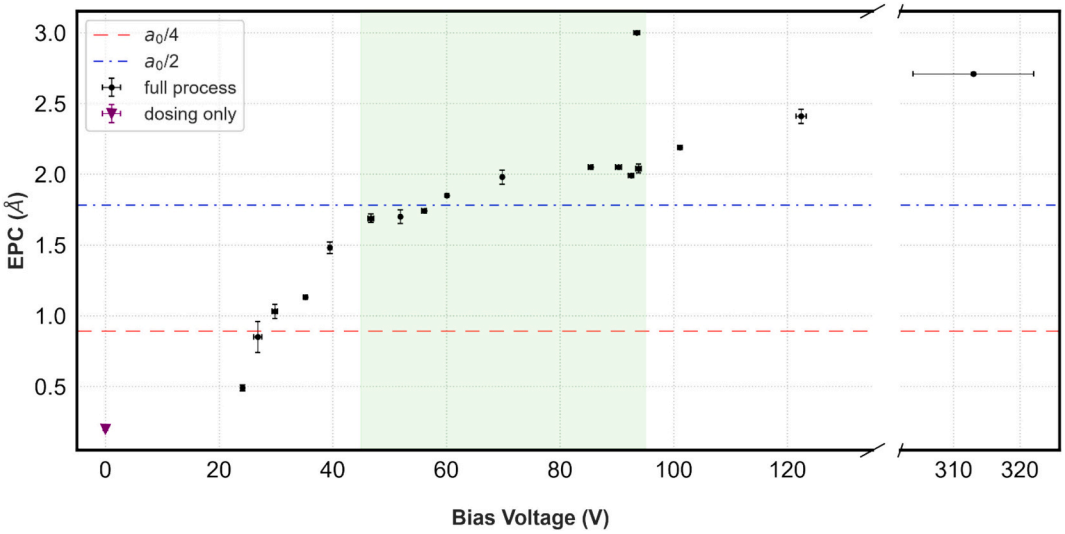


Fig. 2. Etch per cycle obtained for the variation of the table rf power in the etching step (shown as a function of the obtained bias voltage). Between about 45 V and 95 V, we observe the quasi-self-limiting ALE regime (highlighted in green). The red dashed line shows the EPC which would correspond to one atomic layer, the blue dotted-dashed line indicates the EPC corresponding to two atomic layers (half of one unit cell). The triangular data point (purple) is obtained by repeating the experiment without turning on the table rf; it represents the etch per cycle due to the oxygen dosing only. The error bars for the EPC reflect the uncertainty in obtaining the etch depth from the AFM measurements, and the error bars of the bias voltage reflect the variations of the bias voltage read value along the cycles.

95 V bias), we obtain an ALE plateau, meaning, that the complete modified layer is removed without additional sputtering. In the third regime, above about 95 V bias, sputtering of the diamond surface becomes dominant. It is important to add, that the sputter yield of oxygen is much higher than for Argon, which would increase the sputtering much more, if sufficient oxygen is present during the etch step.

For the bias voltage of about 49 V (table rf = 5 W), we determined the synergy of the process, by performing an ALE process of 600 cycles without the dosing step, and an ALE process of the same number of cycles without the etching step. With $\alpha = (0.20 \pm 0.01)$ Å/cycle (etch rate without the Ar Bias) and $\beta = (0.12 \pm 0.01)$ Å/cycle (etch rate without dosing O_2), and using Eq. (1), we obtain a relatively low synergy of $S = (81.01 \pm 0.84)$ %. The EPC of the process obtaining α is also shown in Fig. 2.

A series of etch processes was performed, while keeping the rf table at 5 W and varying the dosing duration from 0 s to 0.70 s. The observed EPCs are shown in Fig. 3. The data resembles the saturation curve of a quasi-self-limiting atomic layer etching process [27]. For the following experiments, the dose duration of 0.25 s was chosen, which is long enough to reach saturation but short enough to minimize the unintentional etching.

In order to study the change of surface topography and the modification of the surface chemistry by the atomic layer etching process, we performed the following experiment: to mimic the surface conditions after the etch mask generation, we performed a triacid cleaning [28] of an as-received sample, followed by thermal evaporation of aluminum. The aluminum was subsequently removed again by in a solution of H_2O:HNO_3:H_3PO_4 (1:1:8) at 50 °C for about 12 min and the sample was subsequently cleaned by rinsing it in water.

AFM measurements on five different 40 μm × 40 μm areas have been performed, in order to obtain a comprehensive roughness analysis of the sample. Furthermore, the surface chemical composition and bonding configuration was investigated by x-ray photoelectron spectroscopy. After performing 600 cycles of the ALE process with table rf 5 W, the same AFM and XPS measurements were performed and the results were compared before and after. Fig. 4 (a) and (b) show representative AFM results before and after the ALE process, Fig. 4 (c) shows the power spectral density (PSD) of a representative line profile perpendicular to

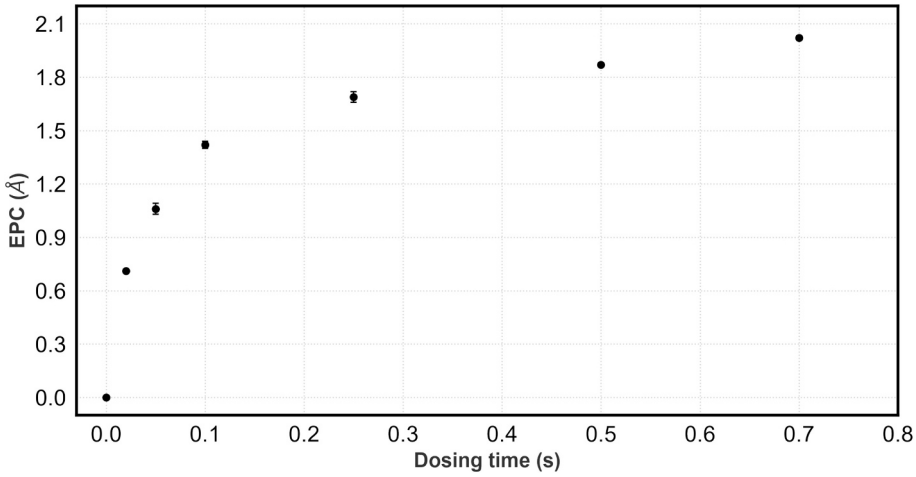


Fig. 3. Variation of dosing time, while using a table rf power for the etch step of 5 W, showing an increase of etch per cycle until a plateau is reached above a dosing time of 0.25 s. The slope of the plateau can be explained by the non-zero etching of the oxygen dosing step.

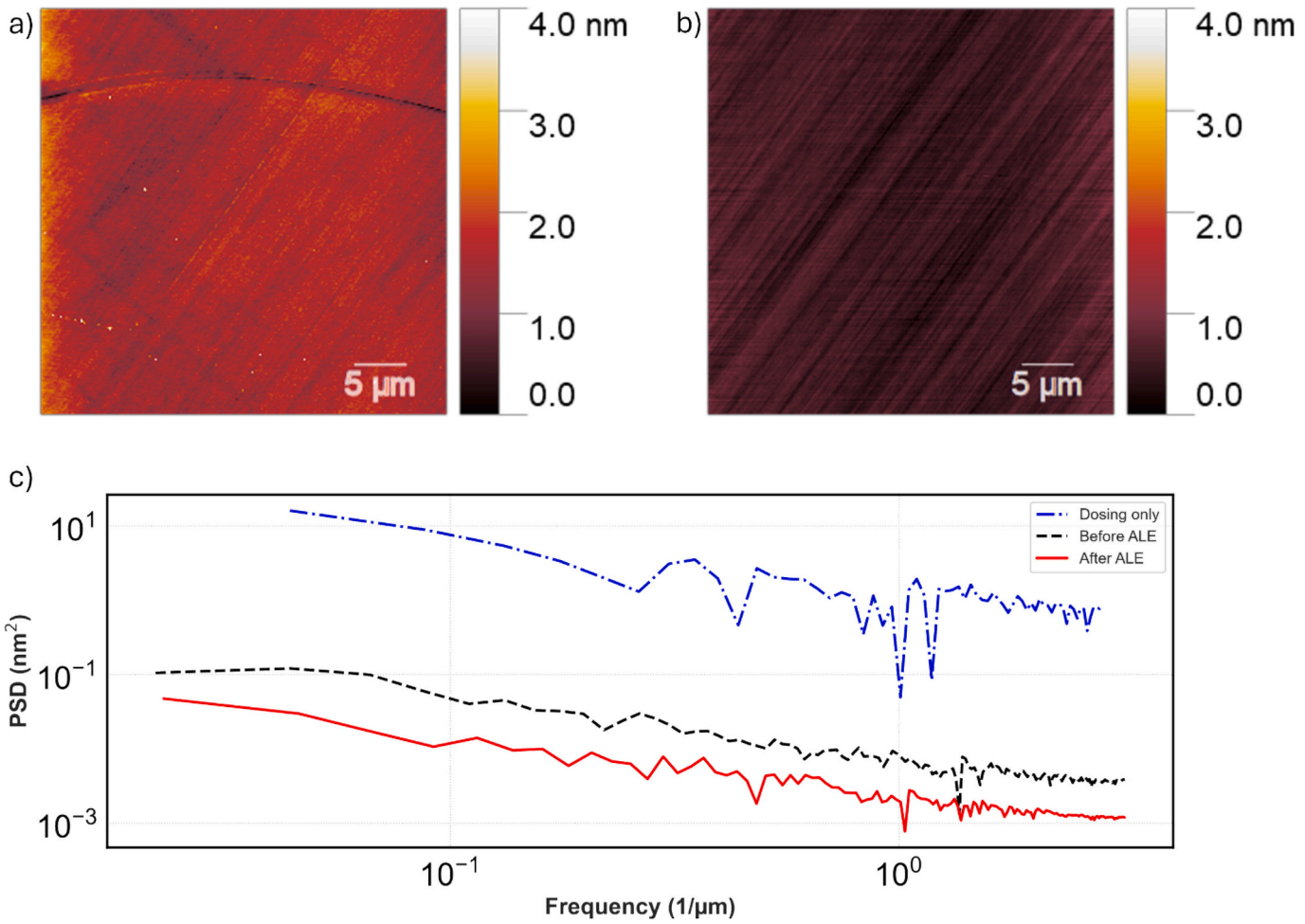


Fig. 4. (a) Representative AFM measurement before the atomic layer etching process, showing polishing lines and small scratches (b) Representative AFM measurement after the atomic layer etching process (c) PSDs obtained from single lines traced perpendicularly to the sample polishing lines. The blue dotted-dashed PSD line is obtained from a different sample and shows the effect on the surface roughness when using oxygen dosing only; the black dashed and solid red lines represent the PSD before and after ALE process at 5 W table rf power. Roughness increases when using oxygen only while decreases after the complete ALE process.

the polishing lines obtained before (black dashed line) and after (red line) the ALE process. The PSD obtained from the etched surface in the process determining alpha (dosing only) is also shown in Fig. 4(c) (as blue dashed-dotted line).

The topographies acquired before the ALE process show differently oriented scratches and ordered polishing lines. Before ALE, the average rms roughness over the scanned areas is (0.26 ± 0.02) nm. After etching, we do not observe the scratches, the average rms roughness is (0.15 ± 0.01) nm. PSD intensity is overall reduced after the ALE process, consistent with a surface roughness reduction on a large range of length-scales.

Chemical characterization before and after the 600 atomic layer etching cycles confirms the presence of carbon and oxygen as the main elemental contributions at the diamond surface. We performed XPS measurements on a sample before atomic layer etching, after the atomic layer etching where the last step was Ar etching, and after the atomic layer etching, when the lasts step was O_2 dosing. At a detection angle of $\theta_1 = 45°$, small elemental residues of Al, Si, P, S, Cl, Na were observed close to the detection limit of the X-ray photoelectron spectrometer (0.1–0.2 at.%) before etching. These contributions possibly originated from masking, cleaning and handling the sample, and mostly vanished after the atomic layer etching process. Trace amounts of P residue remained after etching at reduced quantity (0.1 at.%), the origin remains unclear. After etching, new F and N related residues (0.3 at.% each) were on the surface, close to the detection limit (0.1–0.5 at.%), which are most likely origin from process gas residues of processes run prior in the same process chamber. In accordance to the last etching cycle being the Ar etching, the amount of O was reduced after the 600 atomic layer etching cycles. High-resolution spectra of the C 1s core electron contributions are depicted in Fig. 5, comparing raw data recorded before and after etching. The data displayed was recorded at bulk-sensitive (Fig. 4 (a)) and surface-sensitive (Fig. 5(b)) detection angle. Here, for both detection angles, the overall intensity increased after etching. The integrated intensity of the C—C sp^3 contribution, representing single crystalline bulk diamond, was enhanced by a factor of 1.3 at $\theta_1 = 45°$. An increase of the C—C sp^3 contribution was recorded at $\theta_2 = 70°$ as well, although the effect was less pronounced. The enhanced intensity can hint towards a reduced surface roughness, which is in agreement with the results of the AFM measurements. Peak deconvolution of the C 1s high resolution spectrum at surface sensitive detection angle $\theta_2 = 70°$ is displayed in Fig. 5(c). Displayed spectra show the C 1 s contribution before ALE processing, after the O process step, and after the Ar process step. The main contribution originates from pristine single crystalline diamond C—C sp^3 (284.8 eV). The contribution at lower binding-energy (BE) is identified as C—C sp^2 (283.7 eV) and represents defects of the diamond lattice [29]. The chemical shift of 1.1 eV is in good agreement with reported assignments of C—C sp3 and C—C sp2 [30,31]. The chemical shift of 1.1 eV is in good agreement with reported assignments of C—C sp^3 and C—C sp^2 [30,31]. At higher BE, three contributions were identified and assigned to oxygen single and

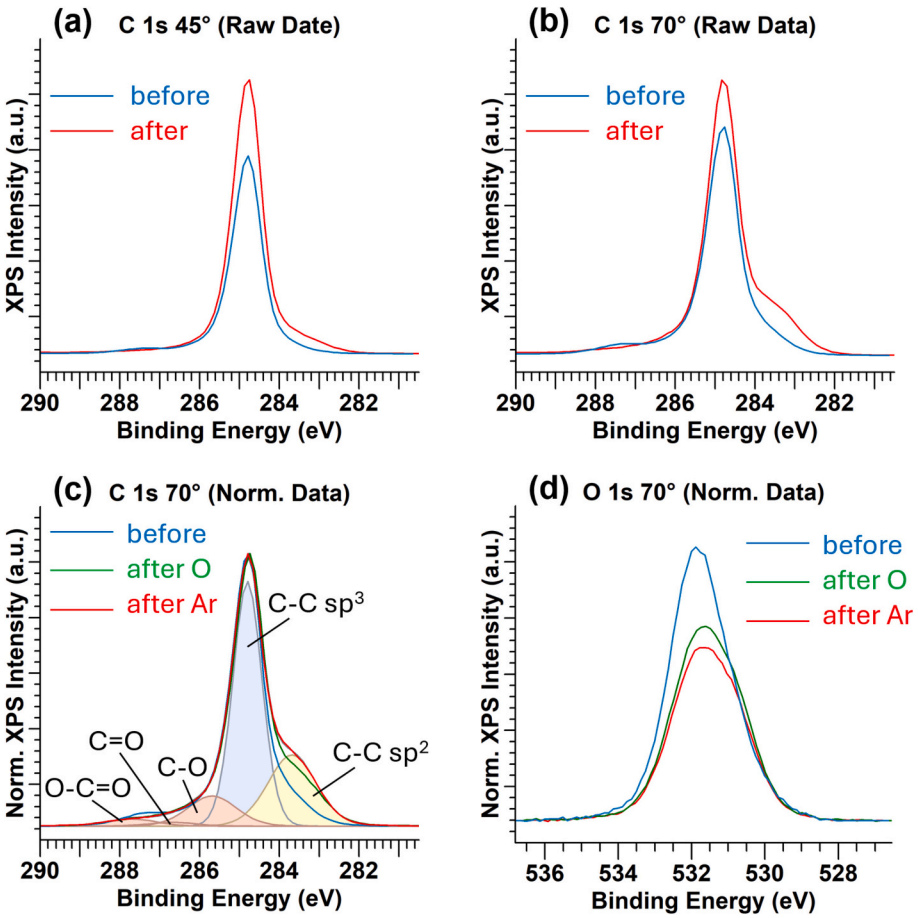


Fig. 5. High-resolution spectra of the C 1s and O1s core electron contribution before and after ALE process. (a)(b) Comparison of C 1s spectra intensities for bulk and surface sensitive detection angle θ, before and after atomic layer etching when the last step was the Ar etch step. After etching the overall spectra intensity increased, hinting at a reduced surface roughness. (c) Comparative display of normalized intensities and peak deconvolution of C 1s high resolution spectra recorded before and after atomic layer etching when the last step is O_2 dosing, and after the atomic layer etching when the last step is the Ar etching step. For easier visualization, peak fitting is included for high-resolution spectra of the C 1s core electron contribution after the final process step only (Ar). The dominant C—C sp^3 bond was accompanied by C—C sp^2 at lower binding energy and oxygen bonded to carbon at higher binding energy. After ALE processing the C—C sp^2 increased, while double bonded oxygen was removed. The highest C—C sp^2 contribution was observed after etching with Ar, (d) Equivalent comparison of ALE process steps, displayed for the O 1s high resolution spectra. Oxygen is clearly removed after atomic layer etching, while the differences in the O 1s intensity is minimal if the last step was O_2 dosing or Ar etching. Some of the measured O most likely originates from atmospheric oxygen adsorbed during sample handling.

double bonded to carbon, namely C—O (285.8 eV), C═O (286.8 eV), and C-O═C (287.8 eV) [32]. For both shoulder-contributions, C—C sp^2 and oxygen bonded to carbon, their relative intensity towards the central C—C sp^3 contribution appears higher at surface-sensitive detection angle than bulk-sensitive detection angle (Fig. 5 (a) (b)). This indicates defects and oxygen bonded to carbon as surface species.

After etching, the intensity for C—C sp^2 and oxygen bonded to carbon in relation to the C—C sp^3 increased. This was evident when O_2 dosing was the last process step and after when Ar etching was the last process step. These changes are especially pronounced for surface sensitive detection, as the intensity of the shoulder at low BE (surface defects) and the shoulder at high BE (oxygen bonded to carbon) of the C 1s contribution is more pronounced at $\theta 2 = 70°$ than $\theta_1 = 45°$ (Fig. 5(a)-(b)). Hence, these changes are confined to the surface of the diamond and direct results of the ALE process itself. This general increase in C—C sp^2 contribution is most likely related to the Ar etching process step, which is breaking surface bonds. The C—C sp^2 contribution measured after the O_2 dosing step is less pronounced, which can be related to O species etching and terminating broken surface bonds. Fig. 5 (c) is displaying the O 1 s high resolution spectrum. Intensities are normalized via the C 1 s contribution. The oxygen amount present on the diamond surface is clearly reduced after ALE processing. This is expected after the Ar etching step, which should remove O species. After the Ar etching step, the oxygen amount on the surface is similar to the oxygen amount after the O_2 dosing step, which can be explained by most of the observed oxygen originating from sample exposure to ambient atmosphere.

In order to demonstrate the feasibility to apply the atomic layer etching process to remove diamond layers while preserving shallow NV centres, we performed the following experiment: one diamond substrate (E6) overgrown by a 100 nm ^{12}C purified diamond layer and subsequently implanted with 5 keV $^{15}N+$ ions (average depth is expected to be around 8 nm [33]), followed by a standard annealing procedure. After 29 ALE cycles (removing about 5 nm diamond from the surface), finishing with a final dosing step, NV centres were still observable, showing a similar Rabi contrast as before the etching, of about 10%. However, a more detailed study on the influence of the atomic layer etching process on the spin properties of shallow NV centres is ongoing.

4. Discussion

We observe a quasi-self-limiting ALE plateau at (1.909 ± 0.004) Å/cycle, which is about half a unit cell of diamond ($a_0/2$ = 3.567 Å/2 = 1.784 Å). In contrast to this, the ALE plateau by the bias-pulsed atomic layer etching process using Cl_2 dosing and Ar etching by Michaels [15] is at around 0.9 Å/cycle, equivalent to one monolayer ($a_0/4$ = 3.567 Å/4 = 0.892 Å). As experimentally indicated [34] and computationally

verified [35], the oxygenated {100} diamond surface can contain both, carbonyl and epoxide groups. Simulations by Enriquez et al. [36] also indicate that, under some conditions, there is a coexistence of carbonyl groups on the first atomic layer and ether groups on the second atomic layer of the {100} diamond surface. The chemisorption of oxygen on {100} diamond is hence a much more complex situation than the chemisorption of chlorine, which is most likely not chemisorbing in more than one configuration to the {100} diamond surface [37,38]. Experimental observations show circumstantial evidence, that oxidative etching of {100} diamond surfaces happens by a layer-by-layer etching process [39,40]. Molecular dynamics simulations furthermore suggest, that {100} diamond surfaces get etched by atomic oxygen even at very low incident energy, and can remove more than one atomic layer at a time [19].

A possible explanation for the observed removal of about two atomic layers per cycle is, that on a clean (100) 2 × 1 reconstructed diamond surface, the chemisorption of oxygen leads to a dereconstruction of the surface, converting the surface dimers into C-O-C (ether) and C═O (carbonyl) sites [36]. It is furthermore known, that surfaces with monolayer oxygen coverage consisting of carbonyl on the first layer and ether on the second layer are structurally stable [34–36]. It can be speculated, that in a situation, where ether and carbonyl structures are next to each other, the Ar ion induced desorption of CO from the ether bridges on the second atomic layer will leave a dangling bond at carbon atoms in the third atomic layer that are connected to the carbonyl structure formed on the first and second atomic layer. Hence, a weakening of the bonds in the third atomic layer could allow the Ar induced desorption of the carbonyl structure on the first and second atomic layer, and therefore lead to the etching of roughly 2 atomic layers at a time. Even though this is a plausible scenario, a verification by e.g. molecular dynamics simulations would be required to uncover the mechanisms leading to the observed results. However, molecular dynamics simulations of the specific scenario of Ar/O_2 atomic layer etching are not known to the authors.

A much higher EPC of about 7.1 Å/cycle, which corresponds to about 2 diamond unit cells, is found by Regnier et al., using a CF_4 dosing and Ar etching [17].

The average kinetic energy of the ions bombarding the substrate E_{Ion} can be roughly approximated as the sum of the plasma potential (V_p) and the measured DC bias ($|V_{Bias}|$), multiplied with the elemental charge: $E_{Ion} \approx q(V_p + |V_{Bias}|)$ [41], where q is the charge of the ions, assumed to be one elemental charge. The plasma potential V_p is typically on the order of 5 V for the PlasmaLab 100 in similar process conditions [42]. Hence, the onset of sputtering is observed approximately at an ion energy of about 100 eV (see Fig. 2). Approximating the sputter threshold E_{th} for diamond bombarded by argon ions, using an empirical sputter yield model [43,44], gives also a value of $E_{th} \approx 70$ eV. A newer, molecular dynamics informed sputter yield model [45] yields a value of $E_{th} \approx 76$ eV. However, the literature data on sputter thresholds of diamond at low energetic ion bombardment is not very consistent, showing no obvious dependency on the various polymorphs of carbon [45]. The similar sputter yield for amorphous carbon and diamond are explained by molecular dynamics simulations by Tran [45] that reveal the bombardment of carbon materials with low energy ions creates an amorphous subsurface, which possesses the same structural characteristics regardless of the initial carbon structure or the sputtering conditions [45]. This may explain, why a lower onset of sputtering of around 75 eV was observed by Kanarik et al. [12] for atomic layer etching of amorphous carbon, but we observe a clear increase of the EPC only above 95 V bias. Hence, it seems that the ALE window is expanding beyond the expected onset of carbon sputtering (70–76 eV). It can be speculated, if the etching process at bias voltages beyond 70 V, where the ion bombardment may be above the sputter threshold of diamond is indeed more like the process described by Draney et al. [18], where amorphized carbon is generated by Ar ion bombardment and afterwards removed by chemical etching by oxygen radicals.

We obtain a synergy of (81.01 ± 0.84) %, which is higher than the synergy obtained for a CF_4/Ar ALE process on diamond by Regnier et al. [17]. Kanarik et al. shows a correlation between the surface binding energy and synergy of ALE processes [12], and for amorphous carbon etched by O_2/Ar, they show a synergy of 97%, much higher than the value obtained by us. The relative low synergy obtained in our process, stems mainly from the slight unintended etching during the dosing step.

The scratches seen on the sample before the ALE process have disappeared afterwards, however, the polishing lines are still visible, but the roughness (rms) is reduced by a factor of 1.7. A reduction of the surface roughness is normally expected to happen during atomic layer etching [24]. The general understanding is that small radii of curvature, having more adsorption sites, may be preferentially etched chemically during the dosing step [24], while ion bombardment of sufficient energy is also known to reduce roughness by promoting diffusion of surface atoms [46]. In contrast to that, a pure etching by an oxygen plasma, as done for the determination of α, is not reducing the roughness, but we observe a severe increase in surface roughness by this process. Since no bias is present, a roughening by micro masking by sputtered Aluminum can be ruled out.

As we see from the angle dependent XPS measurement (Fig. 5a,b), the sp^2 carbon is located on the surface, and not in the bulk. A basic way to estimate an overlayer thickness d from the XPS measurements can be done using [47].

$$d = \lambda_{C1s}\cos(\theta_1)\frac{I_{C1s,overlayer}}{I_{C1s,substrate}} \quad (2)$$

with $\lambda_{C1s} = 2.7$ nm [48], the C 1s electron mean free path in the overlayer, θ_1 the photoelectron emission angle of bulk-sensitive detection, $I_{C1s,overlayer}$ and $I_{C1s,substrate}$ are the integrated intensities from overlayer and substrate core-level contributions, respectively.

In the case, where after the final etch step no termination step was performed, it can be expected that the diamond surface underwent surface reconstruction, and trace oxygen in the chamber, as well as other gas species in the atmosphere are chemisorbed after the sample is exposed to the atmosphere. Free {100} diamond surfaces are known to reconstruct in 2 x 1C(100) surfaces which contain double-bonded carbon dimers [49,50]. Using Eq. (2), we estimate about 1 monolayer of sp^2 bonded carbon for the sample before any etching, about 2.7 monolayers after atomic layer etching with the Ar etching step last, and after the atomic layer etching with oxygen dosing as last step, we obtain about 2.1 monolayers of sp^2 carbon. It is important to mention, that the simple overlayer model used here has its limitations, e.g. by not accounting for the surface roughness, which might also affect the results here. However, we can conclude, that we cannot detect extensive sp^2 formation on the surface after the atomic layer etching process, and that finishing the process with an oxygen dosing step also reduces the surface sp^2 content further.

5. Conclusions

We present and characterize an atomic layer etching process for diamond surfaces, making use of O_2 dosing and Ar etching. An ALE plateau is found at an etch per cycle at about one half of the diamond unit cell. The developed process shows a low synergy of $S = (81.01 \pm 0.84)$ %.

The surface roughness (rms) is diminished by a factor 1.7, which is expected to happen during atomic layer etching [24].

The atomic layer etching process successfully removed trace contaminations from the surface. The removal of double bonded oxygen and the increase of sp^2 bonded carbon on the diamond surface is attributed to the 2 x 1C(100) surface reconstruction. Ending the process with the oxygen dosing step reduces the surface sp^2 content.

The presented possibility to remove defective surface layers by the atomic layer etching process without introducing further surface

damage is an important enabling technology for applications in the fields of quantum computing, quantum sensing, and quantum communications, that make use of shallow color centers in diamond. The presented ability for smoothening the diamond surface without the introduction of an extended defect layer is a key for growing thin, isotopically purified diamond layers with low defect densities on diamond substrates, e.g. for quantum computation or for quantum sensing applications. Future work will be investigating the influence of atomic layer etching on shallow NV centers.

CRediT authorship contribution statement

Alma Beatrice Sergi: Writing – review & editing, Visualization, Methodology, Investigation. **Angelika Kaiser:** Writing – review & editing, Visualization, Methodology, Investigation. **Jakob Buchheim:** Writing – review & editing, Supervision, Resources, Funding acquisition. **Markus Mohr:** Writing – review & editing, Writing – original draft, Supervision, Project administration, Methodology, Investigation, Funding acquisition, Conceptualization.

Declaration of competing interest

The authors declare that they have no known competing financial interests or personal relationships that could have appeared to influence the work reported in this paper.

Acknowledgement

This project was made possible by the DLR Quantum Computing Initiative and the Federal Ministry for Research, Technology and Space; qci.dlr.de/projects/starq. A part of the work was jointly financed by the Ministry of Science, Research and Art, Baden-Württemberg and the Baden-Württemberg Ministry of Economic Affairs, Labour and Tourism as part of QuantumBW. This work was furthermore supported by the Science Sphere Quantum Science of Ulm University. We appreciate the support from Ulm Center for Nanotechnology and Quantum Material. Furthermore, we acknowledge the support by the Core Facility Elemental, Molecular and Materials Analysis at Ulm University.

Data availability

Data will be made available on request.

References

[1] M.W. Doherty, N.B. Manson, P. Delaney, F. Jelezko, J. Wrachtrup, L.C. L. Hollenberg, The nitrogen-vacancy colour centre in diamond, Phys. Rep. 528 (1) (2013) 1–45.
[2] R. Katsumi, K. Takada, F. Jelezko, T. Yatsui, Recent progress in hybrid diamond photonics for quantum information processing and sensing, Commun. Eng. 4 (2025) 85.
[3] S. Steinert, et al., High sensitivity magnetic imaging using an array of spins in diamond, Rev. Sci. Instrum. 81 (2010) 043705.
[4] B.K. Ofori-Okai, et al., Spin properties of very shallow nitrogen vacancy defects in diamond, Phys. Rev. B 86 (2012), 081406(R).
[5] E. Janitz, et al., Diamond surface engineering for molecular sensing with nitrogen – vacancy centres, J. Mater. Chem. C 10 (2022) 13533.
[6] T. Schuelke, T.A. Grotjohn, Diamond polishing, Diam. Relat. Mater. 32 (2013) 17–26.
[7] Pierre-Nicolas Volpe, et al., Defect analysis and excitons diffusion in undoped homoepitaxial diamond films after polishing and oxygen plasma etching, Diam. Relat. Mater. 18 (10) (2009) 1205–1210.
[8] I. Friel, S.L. Clewes, H.K. Dhillon, N. Perkins, D.J. Twitchen, G.A. Scarsbrook, Control of surface and bulk crystalline quality in single crystal diamond grown by chemical vapour deposition, Diam. Relat. Mater. 18 (5–8) (2009) 808–815.
[9] M. Naamoun, A. Tallaire, F. Silva, J. Achard, P. Doppelt, A. Gicquel, Etch-pit formation mechanism induced on HPHT and CVD diamond single crystals by H2/O2 plasma etching treatment, Phys. Status Solidi A 209 (9) (2012) 1715–1720.
[10] A. Denisenko, A. Romanyuk, C. Pietzka, J. Scharpf, E. Kohn, Surface damages in diamond by Ar/O2 plasma and their effect on the electrical and electrochemical characteristics of boron-doped layers, J. Appl. Phys. 108 (2010) 074901.
[11] F.F. de Oliveira, S.A. Momenzadeh, Y. Wang, M. Konuma, M. Markham, A. M. Edmonds, A. Denisenko, J. Wrachtrup, Effect of low-damage inductively coupled plasma on shallow nitrogen-vacancy centers in diamond, Appl. Phys. Lett. 107 (2015) 073107.
[12] K.J. Kanarik, et al., Predicting synergy in atomic layer etching, J. Vac. Sci. Technol. A 35 (2017) 05C302.
[13] L. Zhao, X. Wang, N. Jiang, K. Nishimura, J. Yi, S. Fang, Experimental study of inductively coupled plasma etching of patterned single crystal diamonds, Sci. Rep. 15 (2025) 21062.
[14] S. Iwamatsu, Atomic Layer Etching Method, . Patent JPS5898929A / JPH0379862B2; priority Dec. 9,, 1981.
[15] M.N. Yoder, Atomic layer etching, ", United States Patent 4 756 794, (, 1988.
[16] J.A. Michaels, "Etching for Quantum-Ready Surfaces", PhD thesis, University of Illinois Urbana-Champaign, Illinois, 2023.
[17] M. Régnier, et al., Development of an atomic layer etching process for diamond substrates, J. Vac. Sci. Technol. A 44 (2026) 032602.
[18] J.S. Draney, A.Z. Panagiotopoulos, D.B. Graves, Plasma-assisted atomic layer etching of single-crystal diamond, J. Vac. Sci. Technol. A 44 (2026) 032603.
[19] J. Xu, K. Lu, D. Fan, Y. Wang, S. Xu, M. Kubo, Different etching mechanisms of diamond by oxygen and hydrogen plasma: a reactive molecular dynamics study, J. Phys. Chem. C 124 (2021) 16711–16718.
[20] Y.Y. Kim, W.S. Lim, J.B. Park, G.Y. Yeom, Layer by layer etching of the highly oriented pyrolythic graphite by using atomic layer etching, J. Electrochem. Soc. 158 (12) (2011) D710–D714.
[21] W.S. Lim, Y.Y. Kim, H. Kim, S. Jang, N. Kwon, B.J. Park, J.-H. Ahn, I. Chung, B. H. Hong, G.Y. Yeom, Atomic layer etching of graphene for full graphene device fabrication, Carbon 50 (2012) 429–435.
[22] E. Vogli, D. Metzler, G.S. Oehrlein, Feasibility of atomic layer etching of polymer material based on sequential O2 exposure and Ar low-pressure plasma-etching, Appl. Phys. Lett. 102 (2013) 253105.
[23] https://e6cvd.com/us/application/quantum-radiation/el-sc-plate-2-0x2-0x0-5mm.html, 2026.
[24] K.J. Kanarik, S. Tan, R. Gottscho, Atomic layer etching: rethinking the art of etch, J. Phys. Chem. Lett. 9 (2018) 4814–4821.
[25] David Nečas, Petr Klapetek, Gwyddion: an open-source software for SPM data analysis, Centr. Eur. J.Phys. 10 (1) (2012) 181–188.
[26] N. Fairley, et al., Appl. Surf. Sci. Adv. (2021), https://doi.org/10.1016/j.apsadv.2021.100112.
[27] K.J. Kanarik, T. Lill, E.A. Hudson, S. Sriraman, S. Tan, J. Marks, V. Vahedi, R. A. Gottscho, Overview of atomic layer etching in the semiconductor industry, J. Vac. Sci. Technol. A 33 (2015) 020802, https://doi.org/10.1116/1.4913379.
[28] K.J. Brown, E. Chartier, E.M. Sweet, D.A. Hopper, L.C. Bassett, Cleaning diamond surfaces using boiling acid treatment in a standard laboratory chemical hood, J. Chem. Health Saf. 26 (2019) 6.
[29] G. Alba, M.P. Villar, R. Alcántara, J. Navas, D. Araujo, Surface states of (100) O-terminated diamond: towards other 1 × 1:O reconstruction models, Nanomaterials (Basel, Switzerland) 10 (6) (2020) 1193, https://doi.org/10.3390/nano10061193.
[30] A. Fujimoto, Y. Yamada, M. Koinuma, S. Sato, Origins of sp3C peaks in C1s X-ray photoelectron spectra of carbon materials, Anal. Chem. 88 (12) (2016) 6110–6114, https://doi.org/10.1021/acs.analchem.6b01327.
[31] R. Graupner, F. Maier, J. Ristein, L. Ley, High-resolution surface-sensitive C1s core-level spectra of clean and hydrogen-terminated diamond (100) and (111) surfaces, Phys. Rev. B 57 (19) (1998).
[32] M.C. Biesinger, Accessing the robustness of adventitious carbon for charge referencing (correction) purposes in XPS analysis: insights from a multi-user facility data review, Appl. Surf. Sci. 597 (2022) 153681, https://doi.org/10.1016/j.apsusc.2022.153681.
[33] J.F. Ziegler, SRIM-2003, Nucl. Inst. Methods Phys. Res. B 219–220 (2004) 1027, https://doi.org/10.1016/j.nimb.2004.01.208.
[34] P.E. Pehrsson, T.W. Mercer, Oxidation of the hydrogenated diamond (100) surface, Surf. Sci. 460 (2000) 49–66.
[35] S. Lu, D. Fan, C. Chen, Y. Mei, Y. Ma, X. Hu, Ground-state structure of oxidized diamond (100) surface: an electronically nearly surface-free reconstruction, Carbon 159 (2020) 9–15.
[36] J.I. Enriquez, et al., Oxidative etching mechanism of the diamond (100) surface, Carbon 174 (2021) 36–51.
[37] S. Hadenfeldt, C. Benndorf, Adsorption of fluorine and chlorine on the diamond (100) surface, Surf. Sci. 402-404 (1998) 227–231.
[38] C.J. Widmann, C. Giese, M. Wolfer, S. Kono, C.E. Nebel, F- and cl-terminations of (100) oriented single crystalline diamond, Phys. Status Solidi A 211 (10) (2014) 2328–2332.
[39] F.K. De Theije, N.J. van der Laag, M. Plomp, W.J.P. van Enckevort, A surface topographic investigation of {001} diamond surfaces etched in oxygen, Philos. Mag. A 80 (2000) 725–745.
[40] F.K. de Theije, O. Roy, N.J. van der Laag, W.J.P. van Enckevort, Oxidative etching of diamond, Diam. Relat. Mater. 9 (2000) 929–934.
[41] Thorsten Lill, Atomic Layer Processing - Semiconductor Dry Etching Technology, Wiley-VCH, 2021. ISBN: 978-3-527-34668-4.
[42] S. Dallorto, A. Goodyear, M. Cooke, J.E. Szornel, C. Ward, C. Kastl, A. Schwartzberg, I.W. Rangelow, S. Cabrini, Atomic layer etching of SiO2 with Ar and CHF3 plasmas: a self-limiting process for aspect ratio independent etching, Plasma Process. Polym. 16 (2019) 1900051.
[43] Y. Yamamura, H. Tawara, Energy dependence of ion-induced sputtering yields from monoatomic solids at normal incidence, At. Data Nucl. Data Tables 62 (1996) 149.

[44] H. Tran, H.B. Chew, Threshold energy for sputtering of monoatomic surfaces with noble gas ions, Scr. Mater. 260 (2025) 116590.
[45] H.D. Tran, Material sputtering at low ion energies: from atomistics to engineering models with molecular dynamics, monte carlo, and data-driven approaches, in: Dissertation, Urbana, Illinois, 2024.
[46] D.B. Graves, D. Humbird, Surface chemistry associated with plasma etching processes, Appl. Surf. Sci. 192 (2002) 72–87.
[47] S. Kono, T. Kageura, Y. Hayashi, et al., Carbon 1s X-ray photoelectron spectra of realistic samples of hydrogen-terminated and oxygen-terminated CVD diamond (111) and (001), Diam. Relat. Mater. 93 (2019) 105–130, https://doi.org/10.1016/j.diamond.2019.01. 017.
[48] P.J. Cumpson, M.P. Seah, Elastic scattering corrections in AES and XPS. II. Estimating attenuation lengths and conditions required for their valid use in overlayer/substrate experiments, Surf. Interface Anal. 25 (6) (1997) 430–446, https://doi.org/10.1002/(SICI) 1096-9918(199706)25.
[49] H. Gomez, M.N. Groves, M.R. Neupane, Study of the structural phase transition in diamond (100) & (111) surfaces, Carbon Trends 3 (2021) 100033, https://doi.org/10.1016/j.cartre.2021.100033.
[50] C. Kress, M. Fiedler, W.G. Schmidt, F. Bechstedt, Geometrical and electronic structure of the reconstructed diamond (100) surface, Phys. Rev. B 50 (1994) 17697, https://doi.org/10.1103/PhysRevB.50.17697.